atoms

Article

Optical Lines of Ru^{21+} to Ru^{24+} Ions

Junyu Fan [1,2], Zihuan Jiang [1], Yuyuan Qian [1], Jialin Liu [1], Pengcheng Xu [1], Liangyu Huang [1], Zhencen He [1], Yaming Zou [1], Jiguang Li [3], Chongyang Chen [1] and Ke Yao [1,*]

1 Shanghai EBIT Laboratory, and Key Laboratory of Nuclear Physics and Ion-Beam Application (MOE), Institute of Modern Physics, Fudan University, Shanghai 200433, China
2 Department of Applied Sciences, Delft University of Technology, 2628 CJ Delft, The Netherlands
3 Institute of Applied Physics and Computational Mathematics, Beijing 100088, China
* Correspondence: keyao@fudan.edu.cn

Abstract: In this work, we report a spectroscopy measurement of Ru^{21+} to Ru^{24+} ions in the optical region using a low energy electron beam ion trap. Twelve lines were observed. The multiconfiguration Dirac–Hartree–Fock and relativistic configuration interaction methods were used to calculate the atomic level energies and the transition rates. With the assistance of the theoretical results, eleven magnetic dipole lines were identified. The experimental results provide new reference data for further theoretical investigations of the complex ions.

Keywords: Ru ions; magnetic dipole lines; EBIT; MCDHF

check for updates

Citation: Fan, J.; Jiang, Z.; Qian, Y.; Liu, J.; Xu, P.; Huang, L.; He, Z.; Zou, Y.; Li, J.; Chen, C.; et al. Optical Lines of Ru^{21+} to Ru^{24+} Ions. *Atoms* **2022**, *10*, 154. https://doi.org/10.3390/atoms10040154

Academic Editors: Izumi Murakami, Daiji Kato, Hiroyuki A. Sakaue and Hajime Tanuma

Received: 31 October 2022
Accepted: 14 December 2022
Published: 15 December 2022

1. Introduction

The development of high-resolution spectrograph techniques in the optical region allows us to unambiguously identify the spectral lines emitted from complex highly charged ions and perform high precision measurement. It is valuable in various applications, for instance, diagnostics of properties of terrestrial and astrophysical plasma [1–4], tests of quantum electrodynamics (QED) effects in many electron systems [5,6], and analyses of the atomic level splitting for further developing highly charged ion-based atomic clocks [7–10], etc.

Due to the complex structure of an open $3d$ subshell, strong electron correlation effects exist in the $3d^n$ configurations, in which n is the number of electrons in the $3d$ subshell. Accurate calculations of the atomic energy levels are still challenging, attracting much attention in these systems experimentally and theoretically [11–25]. Great success has been achieved. For instance, a large-scale multiconfiguration Dirac–Hartree–Fock method was used in studying the energy levels of the $3d^n$ (n = 1–9) configurations of tungsten ions [25], and core correlation effects were found to be important. Zhang et al. [19] calculated the $n = 3$ transition energies of W^{47+}–W^{55+} within 0.1% accuracy compared with the experimental value [12] and predicted strong magnetic dipole transition lines in the tungsten ions. However, in the low-Z side, discrepancies between the experimental and calculated results exist [21,23], especially in the $3d^n$ ground configurations. Some significantly large discrepancies were also found along the calcium isoelectronic sequence [21], which hints at the necessity of a reanalysis of the experimental results. In medium heavy ions, very few experiments are available. Experimental reference data are needed for comparisons.

In the case of Ru^{21+}–Ru^{24+} ions, the ground configurations are $3d^5$, $3d^4$, $3d^3$, and $3d^2$, respectively. A number of forbidden transitions connect the energy levels within the ground configurations, part of which correspond to the wavelengths that fall into the optical region. To the best of our knowledge, there are no experimental results available for these ions. In the present work, we reported on the measurement of the magnetic dipole lines from Ru^{21+}–Ru^{24+} ions in a low-energy electron beam ion trap. The corresponding atomic-structure calculations were carried out with the multiconfiguration Dirac–Hartree–Fock

(MCDHF) and relativistic configuration interaction (RCI) methods. With the assistance of the theoretical calculations, eleven observed lines were identified.

2. Experiment

The current experiments were performed in a low-energy electron beam ion trap CUBIT, which has been applied in various measurements of emission lines in highly charged ions [10,14,26]. The operation principle of EBIT has been described in many papers [27–31] in detail. Only a brief description will be given. The CUBIT employs a 0.56 tesla NdFeB permanent magnet to compress the electron beam emitted from a LaB_6 cathode. It usually runs at a few tens of eV to 3 keV, which is sufficient to produce open M-shell ions of medium heavy elements or open N-shell heavy ions. A Wien ion velocity filter is mounted behind the electron collector. The charge state distributions (CSDs) of ions in the trap could be analyzed when extracting the ions in a pulse mode, for unambiguously cataloging the emission lines to the corresponding ions.

The experiment setup was similar to the previous work [14]. In this experiment, the volatile compound $Ru(C_5H_5)_2$ (CAS: 1287-13-4) was continuously injected into the trap region. Ru ions were produced and excited by electron collisions. Light emitted in the decay of the excited ions was focused by a quartz lens mounted outside the vacuum vessel onto the entrance slit of an Andor Shamrock Czerny–Turner spectrometer. The collected light was dispersed by a 1200 mm^{-1} gating and recorded by a charge coupled device. The typical resolving power in the measurement reached about 2700 @427 nm.

A single exposure for one spectrum took two hours, and each line was obtained from the accumulation of at least three exposures to ensure enough statistics and to average out random uncertainties. Line wavelength was calibrated using external Hg, Ar, and Kr lamp reference lines with accurately known wavelength. The validation of the calibration was carefully checked by measuring the emission lines from argon ions with known wavelength.

3. Theoretical Approach

In the present work, the MCDHF and RCI methods were used to calculate the transition energies and transition probabilities. In the MCDHF method, the atomic state function (ASF) is expressed in a linear combination of configuration state functions (CSFs). One of the elaborate tasks in this method is to include the electron correlation effects systematically. The restricted active space method [32–34] was used for this purpose.

For Ru^{24+} ($3d^2$) and Ru^{23+} ($3d^3$), core-valence (CV) correlations were considered by allowing single and double replacements from the $3d$ valance electrons, and single excitation from the $2s$, $2p$, $3s$ and $3p$ core subshells to virtual orbitals with $n \leq 7$ and $l \leq 5$. The main core-core (CC) correlations were also considered by including double replacements from the $3p$ subshell into the same virtual orbitals. The virtual orbitals were expanded layer by layer. To keep the number of CSFs in a controllable size, for Ru^{22+} ($3d^4$) and Ru^{21+} ($3d^5$), only the CV correlations from the $3s$ and $3p$ subshells were included. The virtual orbitals were expanded to $n \leq 7$ and $l \leq 5$ (except $7h$) for Ru^{22+} ($3d^4$), and $n \leq 6$ and $l \leq 5$ for Ru^{21+} ($3d^5$). The numbers of CSFs considered are 853,792, 845,797, 2,230,576 and 595,033 for Ru^{21+}–Ru^{24+}, respectively. The leading QED corrections, namely self-energy and vacuum polarization corrections, and the Breit interaction effect were also included in a followed RCI calculation with the same CSFs described above.

4. Results and Discussion

The nominal electron beam energy varies between 960 eV and 1400 eV to produce the desired ruthenium ions. Due to the complicated charge state distribution evolution in EBIT and the complex atomic structure of the $3d$ subshell, it is difficult to distinguish the ion abundance simply relying on the electron energy, therefore making it difficult for us to identify emission lines. Spectra observation combing a direct CSDs measurement could solve the dilemma, since in the first approximation the line intensity is proportional to the ion abundance.

We take the Ru^{23+} as an example to introduce the procedure briefly. The charge state distributions of Ru ions along with the line intensity are measured at four electron energies as shown in Figure 1. As illustrated in Figure 1a, the line around 426 nm appears when the electron energy exceeds the ionization threshold of Ru^{23+}. Moreover, the line intensity shows an increasing tendency with the CSDs of Ru^{23+} ions (see Figure 1b). As a result, this line is classified as an emission line from Ru^{23+} ions .

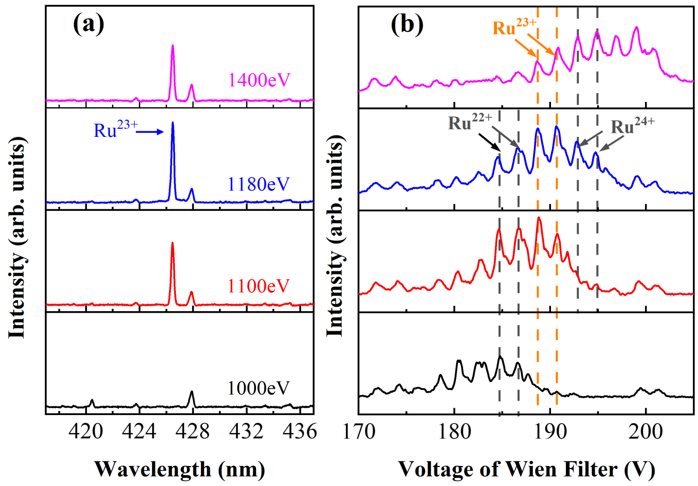

Figure 1. (**a**) Electron beam energy dependence of a transition belonging to Ru^{23+}, (**b**) the corresponding charge state distributions of ruthenium ions. The relationship between the Wien Filter voltage and the ion charge state was calibrated using argon ions in a pre-experiment. The positions of Ru^{22+}–Ru^{24+} are marked with dashed lines. Two separate peaks are resulted from superposition of peaks of different Ru isotopes.

In the same way, spectra of Ru^{21+}–Ru^{24+} ions from 200 to 600 nm are measured, and the wavelengths are determined at the energies in which the abundance of the corresponding ions reach the maximum. In Figure 2, twelve lines in total are observed including four lines from Ru^{21+}, two lines from Ru^{22+}, four lines from Ru^{23+}, and two lines from Ru^{24+}. By comparing with the energies and transition rates calculated with the MCDHF and RCI methods, eleven magnetic dipole lines are identified. As discussed below, the line at 454.730 nm has not been assigned. Experimental and calculated wavelengths (in vacuum) of these transitions are listed in Table 1. The uncertainty (one standard deviation) of each line is listed in the brackets, which consists of three parts, i.e., statistic uncertainties, calibration line uncertainties, and systematic uncertainties caused by the dispersion function. The total uncertainties of these transitions are estimated to be 0.002 to 0.020 nm.

As shown in Table 1, the calculated wavelengths show a good agreement with the experimental results for Ru^{22+}, Ru^{23+}, and Ru^{24+} in general. The deviations are within 1.0% in most cases except for the lines at 338.716 nm and 236.410 nm with the deviation around 2.5%. The deviations of lines from Ru^{24+} are less than 0.3%, which indicates the theoretical model including CV-2s2p3s3p and CC-3p correlations is appropriate. However, we notice that the deviations of lines from Ru^{21+} are as large as 4.5%. Moreover, identification for line at 454.730 nm is still missing. In the Ru^{21+} ($3d^5$) calculation, only the CV correlations from 3s and 3p subshells are included, which may not be adequate to take the main part of correlation effect into account. More complex but efficient theoretical investigations are necessary.

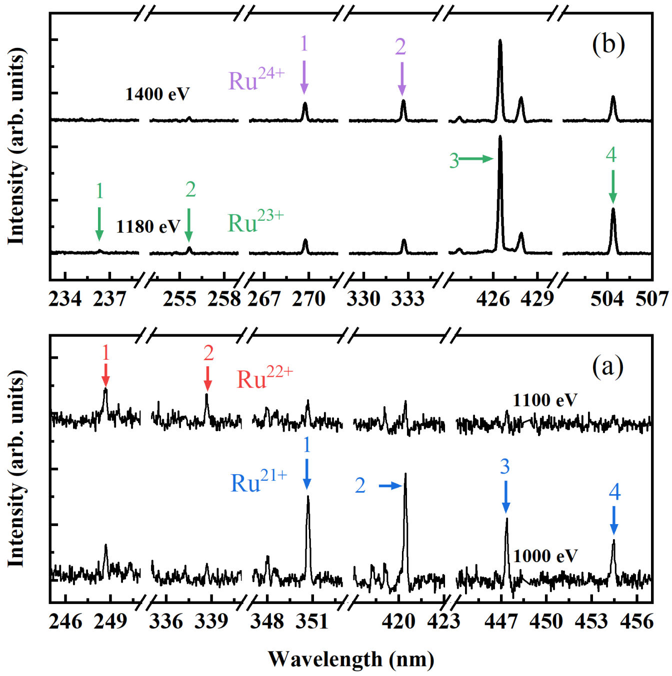

Figure 2. Observed spectra of Ru^{21+}–Ru^{24+} ions. (**a**) Lines of Ru^{21+}, Ru^{22+} at 1000 and 1100 eV, (**b**) lines of Ru^{23+}, Ru^{24+} at 1180 and 1400 eV. The lines labeled with arrows represent the transitions with highest intensity from different ions.

Table 1. Observed forbidden lines of Ru^{21+}–Ru^{24+} ions. Wavelengths (nm, in vacuum) of experimental and calculated results are listed in the column λ_{exp} and λ_{theo}, respectively. The corresponding transitions, transitions rates A, and branch ratios f are also given. The numbers in parentheses denote the uncertainties (one standard deviation), and notation a[b] for transition rates is a $\times$ 10^b. The lable '*' indicates unidentified line.

Ion	Transition	λ_{exp}	λ_{theo}	$A(s^{-1})$	f
Ru^{21+}	$((3d^2_{3/2})_2(3d^3_{5/2})_{9/2})_{7/2} - ((3d^3_{3/2})_{3/2}(3d^2_{5/2})_4)_{7/2}$	350.662(08)	334.863	1.7[2]	0.30
	$((3d^2_{3/2})_2(3d^3_{5/2})_{9/2})_{7/2} - ((3d^2_{3/2})_2(3d^3_{5/2})_{9/2})_{9/2}$	420.370(08)	408.831	7.8[1]	0.13
	$((3d^2_{3/2})_2(3d^3_{5/2})_{9/2})_{7/2} - ((3d^2_{3/2})_2(3d^3_{5/2})_{9/2})_{5/2}$	448.241(05)	430.367	1.8[2]	0.30
	*	454.730(20)			
Ru^{22+}	$((3d^3_{3/2})_{3/2}3d^1_{5/2})_4 - (3d_{3/2}(3d^3_{5/2})_{9/2})_4$	248.853(09)	250.803	4.7[2]	0.78
	$((3d^2_{3/2})_2(3d^2_{5/2})_2)_1 - ((3d^2_{3/2})_2(3d^2_{5/2})_2)_0$	338.716(08)	330.120	4.6[2]	0.11
Ru^{23+}	$(3d_{3/2}(3d^2_{5/2})_4)_{9/2} - ((3d^2_{3/2})_2 3d_{5/2})_{9/2}$	236.410(20)	230.532	8.3[2]	0.54
	$(3d_{3/2}(3d^2_{5/2})_4)_{5/2} - ((3d^2_{3/2})_2 3d_{5/2})_{3/2}$	255.746(08)	256.305	5.6[2]	0.76
	$((3d^2_{3/2})_2 3d_{5/2})_{5/2} - (3d^3_{3/2})_{3/2}$	426.493(04)	430.663	4.4[2]	1.00
	$(3d_{3/2}(3d^2_{5/2})_4)_{7/2} - ((3d^2_{3/2})_2 3d_{5/2})_{5/2}$	504.557(05)	505.204	2.8[2]	1.00
Ru^{24+}	$(3d_{3/2}3d_{5/2})_3 - (3d^2_{3/2})_2$	269.730(02)	270.563	1.1[3]	1.00
	$(3d_{3/2}3d_{5/2})_4 - (3d_{3/2}3d_{5/2})_3$	332.755(02)	332.369	4.9[2]	1.00

To conclude, twelve lines from Ru^{21+}–Ru^{24+} ions are observed at an EBIT. Eleven of these lines are identified by comparing with theoretical calculation results with the MCDHF-RCI methods, and all of these lines are reported for the first time. The unidentified line at 454.730 nm does not correspond with the calculated results. It is most likely that the half-filled 3d shell of Ru^{21+} requires more consideration of electron correlations. The new measurements provide reference data for further atomic structure studies.

Author Contributions: J.F.: investigation, data curation, writing—original draft, formal analysis; Z.J.: investigation, data curation, writing—original draft, formal analysis; Y.Q.: investigation, formal analysis; J.L. (Jialin Liu): data curation, formal analysis; P.X.: investigation; L.H.: methodology; Z.H.: methodology, formal analysis; Y.Z.: methodology, supervision; J.L. (Jiguang Li): validation, supervision; C.C.: software, validation; and K.Y.: investigation, conceptualization, data curation, funding acquisition, project administration, validation, writing—review and editing. All authors have read and agreed to the published version of the manuscript.

Funding: This work is supported by the National Key Research and Development Program of China under Grant No. 2017YFA0402300, the National Natural Science Foundation of China through Grants No. 11874008.

Data Availability Statement: Not applicable.

Conflicts of Interest: The authors declare no conflict of interest.

References

1. Bekker, H.; Hensel, C.; Daniel, A.; Windberger, A.; Pfeifer, T.; López-Urrutia, J.C. Laboratory precision measurements of optical emissions from coronal iron. *Phys. Rev. A* **2018**, *98*, 062514. [CrossRef]
2. Feldman, U.; Curdt, W.; Landi, E.; Wilhelm, K. Identification of Spectral Lines in the 500–1600? Wavelength Range of Highly Ionized Ne, Na, Mg, Ar, K, Ca, Ti, Cr, Mn, Fe, Co, and Ni Emitted by Flares (Te $\geq 3 \times 10^6$ K) and Their Potential Use in Plasma Diagnostics. *Astrophys. J.* **2000**, *544*, 508. [CrossRef]
3. Ding, A.; Habbal, S.R. First detection of prominence material embedded within a 2×10^6 K CME front streaming away at 100–1500 km s^{-1} in the solar corona. *Astrophys. J. Lett.* **2017**, *842*, L7. [CrossRef]
4. Morita, S.; Goto, M.; Katai, R.; Dong, C.; Sakaue, H.; Zhou, H. Observation of magnetic dipole forbidden transitions in LHD and its application to burning plasma diagnostics. *Plasma Sci. Technol.* **2010**, *12*, 341–347. [CrossRef]
5. Draganić, I.; López-Urrutia, J.C.; DuBois, R.; Fritzsche, S.; Shabaev, V.M.; Orts, R.S.; Ullrich, J. High precision wavelength measurements of QED-sensitive forbidden transitions in highly charged argon ions. *Phys. Rev. Lett.* **2003**, *91*, 183001. [CrossRef]
6. Liu, X.; Zhou, X.P.; Wen, W.Q.; Lu, Q.F.; Yan, C.L.; Xu, G.Q.; Xiao, J.; Volotka, A.V.; Kozhedub, Y.S.; Kaygorodov, M.Y.; et al. Precision measurements of the ${}^2P_{1/2} - {}^2P_{3/2}$ fine-structure splitting in B-like S^{11+} and Cl^{12+}. *Phys. Rev. A* **2021**, *104*, 062804. [CrossRef]
7. Windberger, A.; Lopez-Urrutia, J.R.C.; Bekker, H.; Oreshkina, N.S.; Berengut, J.C.; Bock, V.; Borschevsky, A.; Dzuba, V.A.; Eliav, E.; Harman, Z.; et al. Identification of the Predicted 5s-4f Level Crossing Optical Lines with Applications to Metrology and Searches for the Variation of Fundamental Constants. *Phys. Rev. Lett.* **2015**, *114*, 150801. [CrossRef]
8. Bekker, H.; Borschevsky, A.; Harman, Z.; Keitel, C.H.; Pfeifer, T.; Schmidt, P.O.; López-Urrutia, J.R.C.; Berengut, J.C. Detection of the 5p–4f orbital crossing and its optical clock transition in Pr^{9+}. *Nat. Commun.* **2019**, *10*, 5651. [CrossRef]
9. Kimura, N.; Kodama, R.; Suzuki, K.; Oishi, S.; Wada, M.; Okada, K.; Ohmae, N.; Katori, H.; Nakamura, N. Direct determination of the energy of the first excited fine-structure level in Ba^{6+}. *Phys. Rev. A* **2019**, *100*, 052508. [CrossRef]
10. Wang, Y.; Li, Y.; Liu, J.; Jia, F.; Si, R.; Zhang, M.; Huang, L.; Tu, B.; Zou, Y.; Wei, B.; et al. Direct wavelength measurement of the $4p^2\ {}^3P_1 – {}^3P_0$ highly charged ion clock transition in Rh^{13+}. *J. Quant. Spectrosc. Radiat. Transf.* **2022**, *293*, 108370. [CrossRef]
11. Osin, D.; Gillaspy, J.D.; Reader, J.; Ralchenko, Y. EUV magnetic-dipole lines from highly-charged high-Z ions with an open 3d shell. *Eur. Phys. J. D* **2012**, *66*, 1–10. [CrossRef]
12. Lennartsson, T.; Clementson, J.; Beiersdorfer, P. Experimental wavelengths for intrashell transitions in tungsten ions with partially filled 3p and 3d subshells. *Phys. Rev. A* **2013**, *87*, 062505. [CrossRef]
13. López-Urrutia, J.R.C.; Beiersdorfer, P.; Widmann, K.; Decaux, V. Visible spectrum of highly charged ions: The forbidden optical lines of Kr, Xe, and Ba ions in the Ar I to Kr I isoelectronic sequence. *Can. J. Phys.* **2002**, *80*, 1687. [CrossRef]
14. He, Z.; Meng, J.; Li, Y.; Jia, F.; Khan, N.; Niu, B.; Huang, L.; Hu, Z.; Li, J.; Wang, J.; et al. Magnetic-dipole lines in Fe-like and Mn-like Molybdenum ions. *J. Quant. Spectrosc. Radiat. Transf.* **2022**, *288*, 108276. [CrossRef]
15. Silwal, R.; Dipti, D.; Takacs, E.; Dreiling, J.M.; Sers, S.C.; Gall, A.C.; Rudramadevi, B.H.; Gillaspy, J.D.; Ralchenko, Y. Spectroscopic analysis of M- and N-intrashell transitions in Co-like to Na-like Yb ions. *J. Phys. B* **2021**, *54*, 245001. [CrossRef]
16. Suckewer, S.; Hinnov, E.; Cohen, S.; Finkenthal, M.; Sato, K. Identification of magnetic dipole lines above 2000? in several highly ionized Mo and Zr ions on the PLT tokamak. *Phys. Rev. A* **1982**, *26*, 1161–1163. [CrossRef]
17. Morgan, C.A.; Serpa, F.G.; Takács, E.; Meyer, E.S.; Gillaspy, J.D.; Sugar, J.; Roberts, J.R.; Brown, C.M.; Feldman, U. Observation of Visible and UV Magnetic Dipole Transitions in Highly Charged Xenon and Barium. *Phys. Rev. Lett.* **1995**, *74*, 1716. [CrossRef]
18. Watanabe, H.; Crosby, D.; Currell, F.J.; Fukami, T.; Kato, D.; Ohtani, S.; Silver, J.D.; Yamada, C. Magnetic dipole transitions in titaniumlike ions. *Phys. Rev. A* **2001**, *63*,042513. [CrossRef]
19. Zhang, C.; Li, J.; Wang, K.; Si, R.; Godefroid, M.; Jönsson, P.; Xiao, J.; Gu, M.F.; Chen, C. Benchmarking calculations of wavelengths and transition rates with spectroscopic accuracy for W XLVIII through W LVI tungsten ions. *Phys. Rev. A* **2022**, *105*, 022817. [CrossRef]

20. Safronova, M.S.; Safronova, U.I.; Porsev, S.G.; Kozlov, M.G.; Ralchenko, Y. Relativistic all-order many-body calculation of energies, wavelengths, and M1 and E2 transition rates for the $3d^n$ configurations in tungsten ions. *Phys. Rev. A* **2018**, *97*, 012502. [CrossRef]
21. Li, B.; Xu, X.; Chen, X. Relativistic large scale CI calculations of energies, transition rates and lifetimes in Ca-like ions between Co VIII and Zn XI. *Atom. Data Nucl. Data Tables* **2019**, *127–128*, 131–139. [CrossRef]
22. Biémont, E.; Träbert, E.; Zeippen, C.J. Calculated transition probabilities in highly charged Ti-like ions. *J. Phys. B* **2001**, *34*, 1941. [CrossRef]
23. Safronova, U.I.; Johnson, W.R.; Kato, D.; Ohtani, S. Excitation energies and transition rates in the 3d2 states of Ca-like ions. *Phys. Rev. A* **2001**, *63*, 032518. [CrossRef]
24. Feldman, U.; Doron, R.; Klapisch, M.; Bar-Shalom, A. Intensity vs. electron density of the ultraviolet M1 transition in Xe^{32+}, Gd^{42+}, W^{52+}, Bi^{61+}, and U^{70+} (Ti-like ions). *Phys. Scr.* **2001**, *63*, 284. [CrossRef]
25. Fischer, C.F.; Gaigalas, G.; Jönsson, P. Core Effects on Transition Energies for $3d^k$ Configurations in Tungsten Ions. *Atoms* **2017**, *5*, 7. [CrossRef]
26. Li, Y.; Wang, Y.; Fan, J.; Si, R.; Li, J.; Zhang, M.; Huang, L.; Xiao, J.; Zou, Y.; Wei, B.; et al. Precise wavelength determination of the $4s^2 4p\ ^2P_{3/2}$-$^2P_{1/2}$ transition in Mo^{11+} and Ru^{13+} ions. *J. Phys. B* **2021**, *54*,235001. [CrossRef]
27. Levine, M.A.; Marrs, R.E.; Henderson, J.R.; Knapp, D.A.; Schneider, M.B. The Electron Beam Ion Trap: A New Instrument for Atomic Physics Measurements. *Phys. Scr.* **1988**, *157*, T22. [CrossRef]
28. Lu, D.; Yang, Y.; Xiao, J.; Shen, Y.; Fu, Y.; Wei, B.; Yao, K.; Hutton, R.; Zou, Y. Upgrade of the electron beam ion trap in Shanghai. *Rev. Sci. Instrum.* **2014**, *85*, 093301. [CrossRef]
29. Micke, P.; Kuhn, S.; Buchauer, L.; Harries, J.R.; Bucking, T.M.; Blaum, K.; Cieluch, A.; Egl, A.; Hollain, D.; Kraemer, S.; et al. The Heidelberg compact electron beam ion traps. *Rev. Sci. Instrum.* **2018**, *89*, 063109. [CrossRef]
30. Nakamura, N.; Kikuchi, H.; Sakaue, H.; Watanabe, T. Compact electron beam ion trap for spectroscopy of moderate charge state ions. *Rev. Sci. Instrum.* **2008**, *79*, 063104. [CrossRef]
31. Gillaspy, J.D. First results from the EBIT at NIST. *Phys. Scr.* **1997**, *99*, T71. [CrossRef]
32. Roos, B.O.; Taylor, P.R.; Sigbahn, P.E. A complete active space SCF method (CASSCF) using a density matrix formulated super-CI approach. *Chem. Phys.* **1980**, *48*, 157. [CrossRef]
33. Olsen, J.; Roos, B.O.; Jørgensen, P.; Jensen, H.J.A. Determinant based configuration interaction algorithms for complete and restricted configuration interaction spaces. *J. Chem. Phys.* **1988**, *89*, 2185. [CrossRef]
34. Brage, T.; Fischer, C. Systematic calculations of correlation in complex ions. *Phys. Scr.* **1993**, *18*, T47. [CrossRef]